

SUNYAEV–ZEL’DOVICH EFFECT OBSERVATIONS OF STRONG LENSING GALAXY CLUSTERS: PROBING THE OVERCONCENTRATION PROBLEM

MEGAN B. GRALLA^{1,2}, KEREN SHARON², MICHAEL D. GLADDERS^{1,2}, DANIEL P. MARRONE^{1,2,15}, L. FELIPE BARRIENTOS³, MATTHEW BAYLISS^{1,2}, MASSIMILIANO BONAMENTE⁴, ESRA BULBUL⁴, JOHN E. CARLSTROM^{1,2,5,6}, THOMAS CULVERHOUSE⁷, DAVID G. GILBANK⁸, CHRISTOPHER GREER^{1,2}, NICOLE HASLER⁴, DAVID HAWKINS⁷, RYAN HENNESSY^{1,2}, MARSHALL JOY⁹, BENJAMIN KOESTER¹, JAMES LAMB⁷, ERIK LEITCH^{1,2}, AMBER MILLER^{10,11}, TONY MROCZKOWSKI^{12,16}, STEPHEN MUCHOVEJ⁸, MASAMUNE OGURI^{13,14}, TOM PLAGGE^{1,2}, CLEM PRYKE^{1,2,5}, AND DAVID WOODY⁷

¹ Department of Astronomy & Astrophysics, University of Chicago, Chicago, IL 60637, USA

² Kavli Institute for Cosmological Physics, University of Chicago, Chicago, IL 60637, USA

³ Departamento de Astronomía y Astrofísica, Pontificia Universidad Católica de Chile, 7820436 Macul, Santiago, Chile

⁴ Department of Physics, University of Alabama, Huntsville, AL 35812, USA

⁵ Enrico Fermi Institute, University of Chicago, Chicago, IL 60637, USA

⁶ Department of Physics, University of Chicago, Chicago, IL 60637, USA

⁷ Owens Valley Radio Observatory, California Institute of Technology, Big Pine, CA 93513, USA

⁸ Department of Physics and Astronomy, University of Waterloo, Waterloo, Ontario N2L 3G1, Canada

⁹ Space Science Office, VP62, NASA/Marshall Space Flight Center, Huntsville, AL 35812, USA

¹⁰ Columbia Astrophysics Laboratory, Columbia University, New York, NY 10027, USA

¹¹ Department of Physics, Columbia University, New York, NY 10027, USA

¹² Department of Physics and Astronomy, University of Pennsylvania, Philadelphia, PA 19104, USA

¹³ Kavli Institute for Particle Astrophysics and Cosmology, Stanford University, 2575 Sand Hill Road, Menlo Park, CA 94025, USA

¹⁴ Division of Theoretical Astronomy, National Astronomical Observatory of Japan, 2-21-1 Osawa, Mitaka, Tokyo 181-8588, Japan

Received 2010 November 4; accepted 2011 May 17; published 2011 August 8

ABSTRACT

We have measured the Sunyaev–Zel’dovich (SZ) effect for a sample of 10 strong lensing selected galaxy clusters using the Sunyaev–Zel’dovich Array (SZA). The SZA is sensitive to structures on spatial scales of a few arcminutes, while the strong lensing mass modeling constrains the mass at small scales (typically $<30''$). Combining the two provides information about the projected concentrations of the strong lensing clusters. The Einstein radii we measure are twice as large as expected given the masses inferred from SZ scaling relations. A Monte Carlo simulation indicates that a sample randomly drawn from the expected distribution would have a larger median Einstein radius than the observed clusters about 3% of the time. The implied overconcentration has been noted in previous studies and persists for this sample, even when we take into account that we are selecting large Einstein radius systems, suggesting that the theoretical models still do not fully describe the observed properties of strong lensing clusters.

Key words: galaxies: clusters: general – galaxies: clusters: intracluster medium

1. INTRODUCTION

Earlier studies have found that strong lensing galaxy clusters are more concentrated than simulations predict (e.g., Broadhurst et al. 2005, 2008b; Oguri et al. 2005; Hennawi et al. 2007). Early forming halos are more concentrated (e.g., Wechsler et al. 2002), so this discrepancy could be explained if dark matter halos form at earlier times than the standard Λ CDM prediction. Exotic physics such as non-Gaussianity or early dark energy could cause such an early collapse of dark matter halos (e.g., Mathis et al. 2004; Fedeli & Bartelmann 2007). Another explanation for the observed overconcentration could be that current models do not properly incorporate the effects of baryons on the core density profiles in clusters (e.g., Rozo et al. 2008). The discrepancy could also result from inaccuracies in current cluster models of strong lenses due to extrapolations of the concentration probability distribution from more easily simulated, lower mass systems (discussed in Oguri & Blandford 2009).

Broadhurst & Barkana (2008a) recast this overconcentration problem into a comparison of the cluster mass at small scales with the cluster mass at large scales. They measured the inner mass through strong lensing mass modeling and expressed it in

terms of the Einstein radius, θ_E , which for a circularly symmetric lens with an arbitrary mass profile satisfies $\theta_E^2 \propto M(<\theta_E)$ (Narayan & Bartelmann 1997). They measured the overall cluster mass through weak lensing. This approach is useful because it enables a comparison to theoretical predictions without measuring the concentration of the cluster profile, which would require knowledge of the shape of the density profile over a wide range of scales in the cluster, some of which are not well constrained by the available data. For a sample of four strong lensing clusters, they found mass measurements that are discrepant with theoretical predictions and interpreted this disagreement as a conflict between their observations and Λ CDM cosmology. However, the sample size was not large, and they did not fully account for the selection of large Einstein radius systems from the rather wide expected distribution of Einstein radii when determining the significance of the discrepancy.

Other authors have constructed strong lensing models for larger samples of massive clusters, often selected on the basis of other mass proxies, such as X-ray luminosity, rather than as strong lenses. These studies also find that the distribution of measured Einstein radii is larger than expected, although the significance of the discrepancy is small (Smith et al. 2005; Zitrin et al. 2011). Until now, there has not been a similarly large sample of well-studied, specifically strong lensing selected

¹⁵ Hubble Fellow.

¹⁶ Einstein Fellow.

clusters. Because most of the larger samples are either X-ray selected or a combination of X-ray and strong lensing selected, it is typically difficult to get spectroscopic redshifts for their relatively faint arcs, although spectroscopic redshifts are very useful for constraining the strong lensing mass models. It is also less clear how these samples compare to a sample of halos selected from simulations as efficient strong lenses.

Using the Sunyaev–Zel’dovich Array (SZA), we have observed the Sunyaev–Zel’dovich (SZ) effect for a sample of 10 clusters selected from large optically selected cluster catalogs for their strong lensing signatures. We derive mass measurements from these SZ observations and Einstein radii measurements from detailed strong lensing mass modeling, comparing our results with theoretical predictions. A strength of using intracluster-medium-based mass estimates for strong lensing clusters is that they have less scatter at fixed mass than optical richness measurements and different dependencies on line-of-sight structure than weak lensing measurements (strong lenses are expected to be preferentially aligned along the line of sight). This paper is part of a larger program to obtain a variety of mass estimates for strong lensing clusters (weak lensing, velocity dispersion, X-ray).

Throughout this work, we assume a flat Λ CDM cosmology with $\Omega_m = 0.27$, $\Omega_\Lambda = 0.73$, and $h = 0.73$ in order to calculate the angular diameter distances to the clusters and sources. The theoretical models are derived adopting the WMAP5 cosmology as the fiducial cosmological model (Dunkley et al. 2009).

2. DATA AND ANALYSIS

2.1. Sample Selection

We select strong lensing clusters from two programs: the Sloan Giant Arc Survey (SGAS) and the Red-Sequence Cluster Survey Giant Arc program (RCS-GA). The selection of strong lensing clusters for SZA observations was driven by right-ascension constraints and availability of complementary data (primarily spectroscopy to facilitate lens modeling).

SGAS is a survey to detect strong lensing by clusters with the clusters selected via the red-sequence method (Gladders & Yee 2000) applied to the Sloan Digital Sky Survey (SDSS) DR7 (Abazajian et al. 2009) photometry. Lenses have been selected in two ways: either by imaging of rich clusters to search for lensing features (Hennawi et al. 2008) or from clusters and groups (not necessarily rich) that show evidence for lensing directly in the SDSS imaging (M. D. Gladders et al. 2011, in preparation). Candidates were subsequently confirmed by further imaging. In either case, deeper imaging was obtained at the Wisconsin–Indiana–Yale NOAO 3.5 m telescope, the University of Hawaii 88 inch telescope, or the 2.5 m Nordic Optical Telescopes. SGAS targets in this paper are drawn from both samples.

The RCS-GA is a program to detect strong lensing around clusters in the second Red-Sequence Cluster Survey¹⁷ (RCS2; Gilbank et al. 2011). RCS2 clusters are also selected photometrically using the red-sequence method. The survey covers nearly 1000 deg², with imaging in g' , r' , z' filters from the Canada–France–Hawaii Telescope. The typical 5σ point source depth is 25.3 mag in the g' band, 24.8 mag in the r' band, and 22.5 mag in the z' band. Strong lensing features were identified by eye from three-color composite images of clusters directly from the survey data.

Because arc redshifts are important for constraining strong lensing mass models, we only selected strong lenses with spectroscopically measured arc redshifts. We supplemented our sample with two additional clusters from the literature, one from the first Red-Sequence Cluster Survey (RCS1), RCS1J2319, and a well-known strong lensing Abell cluster, A1689. Table 1 contains information about the sample.

2.2. SZ Observations and Analysis

The SZA is an eight-element interferometer originally located at the Owens Valley Radio Observatory in California that is now incorporated into the Combined Array for Research in Millimeter-wave Astronomy (CARMA) at a nearby 2200 m elevation site at Cedar Flat in the Inyo Mountains of California. All of the observations were conducted at a center frequency of 31 GHz, for which the SZA has baselines of 350–1300 λ , corresponding to spatial scales¹⁸ of 9'.8–2'.6 for sensitivity to the cluster SZ effect and baselines of 2–7 k λ for the simultaneous measurement of compact radio sources. Radio sources were found within 1 arcmin of the target center for 7 out of the 10 targets. The on-source, unflagged observing time for each cluster ranged from 11 to 57 hr and resulted in rms noise of 0.23–0.08 mJy beam⁻¹ for the short baselines. Muchovej et al. (2007) provide a detailed description of the SZA instrument, measurements, and the data reduction pipeline developed by the SZA collaboration.

We use Markov Chain Monte Carlo (MCMC) analysis software (Bonamente et al. 2004) to fit a model for the gas pressure to the visibility data. The model is based on the Nagai et al. (2007) simulations with parameters fit to X-ray data. The pressure profile is given by

$$P(r) \propto x^{-\gamma}(1+x^\alpha)^{-(\beta-\gamma)/\alpha}, \quad (1)$$

where $x \equiv r/r_s$, where r_s is the scale radius of the profile, and with parameters α , β , and γ set to 0.9, 5.0, and 0.4, respectively. Mroczkowski et al. (2009) found that this model fits both SZ and X-ray data well. For each cluster, we determined the best-fit parameters for the pressure profile normalization and scale radius and used these in all subsequent analyses. The fluxes of compact radio sources were fit along with the cluster parameters.

The observable from the SZ effect is the integrated Compton y -parameter, Y , which is proportional to the integrated pressure of the intracluster gas. We calculate a spherically integrated SZ parameter, $Y_{500,\text{sph}}$, by integrating the pressure profile to r_{500} , defined as the radius within which the enclosed mass is equal to 500 times the critical density of the universe. We chose this radius to use available scaling relations (see Table 1).

Masses are calculated from the integrated Y ; we used a scaling relation based on SZA observations and weak lensing measurements of clusters in the Local Cluster Substructure Survey¹⁹ (LoCuSS) sample. Details of the LoCuSS sample will be found in G. P. Smith et al. (2011, in preparation), and details of the weak lensing analysis are found in Okabe et al. (2010). The LoCuSS SZ measurements and analysis will be published in an upcoming paper (D. P. Marrone et al. 2011, in preparation). The LoCuSS clusters span a similar range in integrated Y (when scaled by $E(z)^{-2/3}$, as expected for self-similar scaling) as the strong lensing clusters, although they lie at lower redshifts. We

¹⁸ This refers to the wavelength of the Fourier component measured; the largest features imaged well in a map are about a factor of two smaller.

¹⁹ <http://www.srbham.ac.uk/locuss>

¹⁷ <http://rcs2.org>

Table 1
Strong Lensing Cluster Sample

Name	Cluster z^a	r_{500} ($''$)	r_{500} (Mpc)	Y_{sph} (10^{-5} Mpc^2)	M_{500} $\times 10^{14} M_{\odot}$	Arc z^a	θ_E ($''$)	θ_E for $(z_l, z_s) = (0.5, 2.0)$ ($''$)	Lensing Reference ^b
A1689	0.18	503	1.5	$24.8^{+6.5}_{-4.9}$	$10.9^{+2.1}_{-1.9}$	1.100 3.000 4.800	42.6 52.3 54.4	40.2 ± 2.0	1
A1703	0.28	251	1.0	$4.6^{+1.1}_{-0.8}$	3.9 ± 0.7	0.880 3.380	19.2 31.3	32.5 ± 1.9	2
A963	0.21	321	1.1	$4.4^{+1.1}_{-0.8}$	$3.9^{+0.7}_{-0.6}$	0.771 1.958	6.7 16.5	$18.5^{+2.3}_{-6.2}$	3
RCS1 J2319	0.90	85	0.6	$1.5^{+0.6}_{-0.5}$	2.0 ± 0.4	3.860	12.9	$12.8^{+4.7}_{-2.0}$	3
RCS2 J0327	0.56	133	0.8	$2.8^{+0.4}_{-0.5}$	2.7 ± 0.4	1.701	21.8	25.3 ± 1.5	4
RCS2 J2327	0.70	155	1.1	12.3 ± 0.7	6.5 ± 0.8	1.415 2.983	25.9 39.6	$34.4^{+2.8}_{-2.1}$	3
SDSS J1209+26	0.56	161	1.0	$7.3^{+2.6}_{-1.9}$	$4.9^{+1.1}_{-1.0}$	1.018 3.949	8.3 27.3	23.0 ± 1.4	3
SDSS J1343+41	0.42	134	0.7	$0.9^{+0.4}_{-0.3}$	1.6 ± 0.4	2.090 5.200	15.2 20.9	$14.1^{+1.2}_{-0.9}$	5
SDSS J1531+34	0.34	164	0.8	$1.1^{+0.3}_{-0.2}$	$1.7^{+0.4}_{-0.3}$	1.096	12.3	$18.0^{+2.0}_{-1.8}$	3
SDSS J2111-01	0.64	109	0.7	$2.3^{+0.3}_{-0.4}$	2.3 ± 0.4	2.861	16.2	$14.4^{+3.5}_{-6.0}$	3

Notes.

^a Cluster and arc redshift references are Limousin et al. (2007, 2008) and references therein for A1689, A1703, respectively; Smith et al. (2005) and references therein for A963, Gilbank et al. (2008) for RCS1 J2319, Wuyts et al. (2010) for RCS2 J0327, and information on RCS2 J2327 will be published in M. D. Gladders et al. (2011, in preparation). All other cluster and arc redshifts are published in Bayliss et al. (2011).

^b Lens model references are: (1) Limousin et al. 2007; (2) Limousin et al. 2008; (3) K. Sharon et al. 2011, in preparation; (4) Wuyts et al. 2010; (5) Bayliss et al. 2010.

fixed the slope of the scaling relation to the self-similar value of 0.6. Lacking a priori knowledge of the radius r_{500} , we iteratively solve for r_{500} and M_{500} through the scaling relation; for each iteration we integrate the pressure profile to the r_{500} from the previous iteration to calculate Y_{sph} , then calculate M_{500} from the scaling relation, calculate r_{500} according to this M_{500} , and repeat until this converges, typically after about four steps. See Table 1 for the resulting r_{500} , $Y_{\text{sph},500}$, and M_{500} for each cluster in this sample.

2.3. Lensing Mass Models

Einstein radii for the clusters in this sample were computed from strong lensing models that were either derived for this work or taken from the literature (Table 1). When taken from the literature, the models were adjusted according to our fiducial cosmology. All the lensing models that are utilized here were constructed using the publicly available software `lenstool` (Jullo et al. 2007), with MCMC minimization in the source plane. A detailed description of the lens modeling process will be published elsewhere (K. Sharon et al. 2011, in preparation). In short, we consider only clusters with secure spectroscopic redshifts for both the cluster and at least one source. The redshifts and positions of multiply imaged arc systems (sources) are used as constraints, and when available, cluster velocity dispersions and low-uncertainty photometric redshifts of secondary arcs are used as priors. The clusters are typically modeled with several mass halos, depending on the complexity that is needed: a Navarro et al. (1997, NFW) or pseudo-isothermal ellipsoid mass distribution (PIEMD) to represent the cluster mass; a secondary PIEMD to represent a group-scale halo or external shear; and contributions from cluster-member galaxies, represented by PIEMDs, with parameters that follow their observed values and scale with luminosity (see Limousin et al. 2007).

The model-inferred Einstein radius is defined as $\theta_E = \sqrt{A}/\pi$, where A is the area inside the tangential (outer) critical curve.

For an elliptical critical curve, this is equivalent to the definition that Oguri & Blandford (2009) used; we have simply generalized it to more complex lensing models.

To compare the observed Einstein radii for clusters of different redshifts to theoretical predictions, we recompute θ_E of each cluster as follows. For each cluster, we derive a lensing mass reconstruction as explained above, according to the measured cluster and arc redshifts. We then use the derived mass distribution, assign to it the fiducial cluster redshift of 0.5 (near the average cluster redshift of the sample), and compute θ_E for a source plane at $z = 2.0$. The resulting Einstein radii for the actual cluster and source redshifts as well as for the fiducial ones are listed in Table 1.

The uncertainties of the model-dependent Einstein radii are estimated through simulation. For each cluster, we compute θ_E in a series of lens models, each one with a set of parameters drawn from steps in the MCMC that are within $[\chi_{\text{min}}^2, \chi_{\text{min}}^2 + 2]$. For most of the clusters, the simulated θ_E values differ from that of the best-fit model by less than 5%, although there are a few notable exceptions. RCS1J2319 and SDSS2111-01 are only constrained by arcs that lie on one side of the cluster center. This means that although the critical curves in all the accepted models are tightly constrained to pass through these arcs, a variety of critical curve shapes and sizes are allowed by the data, resulting in larger uncertainties on the θ_E values (up to $\sim 40\%$). In the case of A963, the cluster mass is degenerate with the position of the cluster centroid, resulting in a similarly large uncertainty in θ_E (33%).

As noted above, the location of the critical curve is directly determined by observations. If we were to use in our analysis θ_E as derived for the actual cluster and arc redshifts, the uncertainties estimated above would be satisfactory. However, for some clusters the extrapolation of the models to the fiducial redshift may result in an additional uncertainty. K. Sharon et al. (2011, in preparation) show that the total projected mass inside

the critical curve can be measured to within a few percent, even with a limited number of multiply lensed images—as is the case with most of the clusters in this sample. However, outside the range of radii in which arcs are observed, the enclosed mass becomes uncertain. Assuming that $M(<\theta_E) \propto \theta_E^2$ (Narayan & Bartelmann 1997) and thus $\Delta M(<\theta_E)/M(<\theta_E) \propto \Delta\theta_E/\theta_E$, we argue that the accuracy with which θ_E is known is only as good as the accuracy of the enclosed mass.

We therefore examine each R_E with respect to the observed projected distances of the arcs in each cluster. In all but three clusters, the fiducial R_E is within the radial range covered by observed arcs. For these clusters we conservatively increase the relative uncertainty of R_E by 5%. For the other three clusters, A963, SDSS J1343, and SDSS J1531, we increase the relative uncertainty by 5.5%, 5.5%, and 8.9%, respectively, based on the relative scatter in mass measurement as a function of radius from K. Sharon et al. (in preparation).

2.4. Theoretical Predictions

Oguri & Blandford (2009) calculated the expected distributions of large Einstein radii for triaxial dark matter halos based on a semi-analytic model. They randomly generated a catalog of massive dark matter halos according to a mass function, assigning each halo a density profile following a triaxial generalization of the NFW profile, with the axis ratio and concentration parameter randomly assigned according to the probability distributions determined by N -body simulations of dark matter halos in Jing & Suto (2002). They projected these triaxial halos in two dimensions and calculated the resulting projected convergence and shear maps. Einstein radii were defined as the geometric mean of the distances from the halo center to the outer critical curve along the major and minor axes of the projected two-dimensional density distribution. They produced 300 realizations of these mock all-sky catalogs of Einstein radii. For further details, see Oguri & Blandford (2009).

Based on these models, we generate an average relation between the Einstein radii and M_{500} for a large Einstein radius sample cluster population for the same fiducial lens and source redshifts that are used to calculate the Einstein radii (0.5 and 2.0, respectively). This effectively is a measure of the projected concentration, but using the two observables corresponding to the two different measurements we made for our real sample of clusters. We have not included the expected redshift evolution in the concentrations of halos (which goes as $c_{2D} \propto (1+z)^{-0.71}$; Duffy et al. 2008). However, the evolution is not strong, and because our fiducial redshift lies near the sample median redshift, this does not introduce a significant bias.

A strong lensing selected sample tends to have larger Einstein radii than a sample selected based on other mass observables. We have included this selection effect in the predictions for the relation between the Einstein radii and M_{500} by weighting the probability distribution of the Einstein radius at a given mass with the square of θ_E , which is proportional to the lensing cross section. We note that the average Einstein radius is not noticeably affected by including a brightness cut on the arcs that mimics our selection.

3. RESULTS AND DISCUSSION

3.1. Mass and Einstein Radius

The main result of this paper is shown in Figure 1. This figure shows M_{500} , as derived from SZ measurements, versus Einstein radius for this sample of strong lensing selected galaxy clusters.

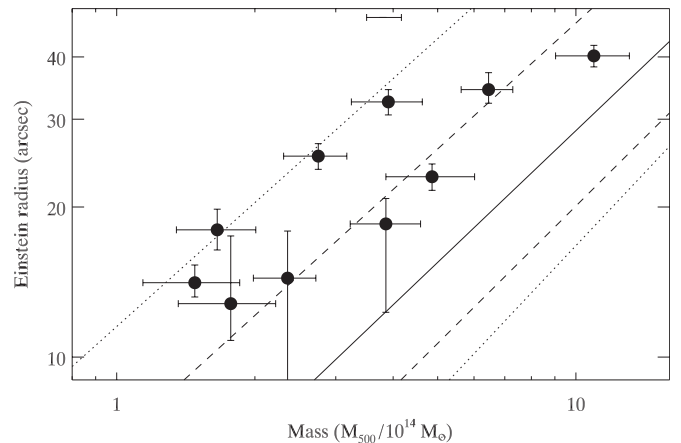


Figure 1. Einstein radii vs. M_{500} (as derived from SZ measurements) for strong lensing clusters. The solid line shows the median of the theoretical halo models that have been selected to be efficient strong lenses. The dashed lines enclose 68% of such models, and the dotted lines enclose 90%. All of the lensing models have been scaled to a fiducial lens redshift of 0.5 and a fiducial source redshift of 2.0. The error bar at the top of the plot shows the median uncertainty in mass from the uncertainty in the normalization of the scaling relation used to determine the masses from the SZ observations.

The solid line shows the median of the theoretical halo models that include lensing selection. The dashed lines enclose 68% of such models, and the dotted lines enclose 90%. The uncertainties on the masses are calculated by adding in quadrature the statistical error on the Y measurement as determined by the Markov chain with the scatter at a given mass in the mass–observable relation. There is an additional systematic uncertainty on the iteratively determined masses that results from the uncertainty in the normalization of the scaling relation used to determine the masses, represented in Figure 1 by an error bar at the top of the figure. As expected, clusters with larger Einstein radii tend to have larger observed masses. The data fall within the theoretically expected distribution, although on average, clusters of a given mass have Einstein radii twice as large as expected, or alternatively the masses measured from the SZ effect are expected to be about twice as high as observed.

To better quantify the level of agreement between the data and the theoretical predictions, we generate a Monte Carlo simulation, populated by drawing masses from the masses of the clusters observed (varied by their uncertainties) and calculating the corresponding Einstein radii according to the theoretically expected distribution. We modeled this distribution as a four-part piecewise lognormal distribution for Einstein radius at fixed mass with the widths set to approximate the 68% and 90% levels shown in Figure 1. The slope as a function of mass was set by the median relation. We vary the Einstein radius measurements by their associated uncertainty, and we include a cut so that the Einstein radii are all greater than $12''.5$ to account for any Malmquist bias effects. For each Monte Carlo realization, we calculate the difference between the Einstein radii of that realization and the theoretically expected Einstein radii. A sample with a median difference greater than we observe was measured for 2.8% of the realizations. While on average our data do not agree with the models, they do lie within the 90% region of the models, so we are not extrapolating far beyond the regions where the models lie. A probability tail to large Einstein radii that could potentially explain our observations is not currently captured by this model, which is based on simulations and includes a prescription for halo triaxialities and concentrations.

The uncertainty in the amplitude of the scaling relation used to calculate mass from the SZ observations results in an uncertainty in the masses that is correlated across the sample. This affects the above calculation, such that the probability of selecting from the Monte Carlo simulation a sample as observed ranges from 2.4% to 4.4% when the scaling relation normalization is varied by its 1σ statistical uncertainty.

3.2. Potential Systematic Effects

One concern in this analysis is that the properties which make a cluster a more efficient strong lens could also bias the mass measurement derived from the SZ effect. Hennawi et al. (2007) identified strong lenses in simulations and found that strong lensing clusters are preferentially aligned along the line of sight compared to the general halo population. This could introduce a bias in our mass determinations when we fit a spherical model to the SZ data and then use a scaling relation derived from halos that are expected to be more randomly oriented. When we simulate SZA data for projected triaxial models and fit a pressure model to these data, we find that for clusters for which the scale radius is smaller than the largest scales to which the SZA has sensitivity (all strong lensing clusters except for Abell 1689), the spherically integrated Y_{500} calculated is higher for an elongated halo aligned along the line of sight than for the same halo oriented in the plane of the sky. Applying the scaling relation, which was derived for clusters that were not selected to be strong lenses, could cause us to overestimate the masses. Another possibility is that an active merger could enhance a cluster's probability for strong lensing (Torri et al. 2004), which could also inflate the pressure and lead to an overestimate in the SZ mass derived from the scaling relation. If these systematic effects are important, then we are underestimating the discrepancy between the observations and theory, such that our quoted results would be conservative.

The scaling relation used to measure the mass from the SZ integrated Y parameter is based on weak lensing measurements of X-ray selected clusters. Using simulations, Meneghetti et al. (2010) found that on average X-ray mass measurements are biased toward low values (by $\sim 5\%$ – 10%), and weak lensing mass measurements have larger scatter (up to $\sim 20\%$) than X-ray mass measurements. However, because we are basing the SZ mass measurements not on the assumption of hydrostatic equilibrium, but on a scaling relation with weak lensing, we would not expect the same bias Meneghetti et al. (2010) found in the hydrostatic mass estimates to affect the SZ masses.

Another possibly important systematic effect could result from our use of the scaling relation based on the LoCuSS sample if the gas fraction, f_{gas} , for LoCuSS clusters is significantly different than the typical gas fraction of the clusters in the strong lensing sample. Hicks et al. (2008) conducted X-ray observations of a sample of high redshift ($0.6 < z < 1.1$) optically selected clusters from RCS1 and calculated the hydrostatic masses and gas fractions as well as the X-ray equivalent of the integrated Y parameter, Y_X . They found that the gas fraction at M_{500} for high redshift ($0.6 < z < 1.0$) optically selected galaxy clusters is lower on average than for lower redshift, X-ray-selected clusters and also lower than theoretical predictions. This affects the normalization of the scaling relation between the hydrostatic mass and Y_X .

To investigate what effect this would have on our analysis, we convert the $Y_{\text{sph,SZ}}$ for the LoCuSS clusters to the equivalent Y_X according to the scaling relation from Andersson et al. (2010) that allows a free slope and no evolution, and we recalculate

the $Y - M$ scaling relation based on the weak lensing masses, fixing the slope to the self-similar value (which is equivalent to the slope for the $Y_X - M$ scaling relation from Hicks et al. 2008). We compare the normalization of this scaling relation with the normalization of the scaling relation derived for the optically selected clusters by Hicks et al. (2008). The difference in normalization is about 0.4 in M at fixed Y , indicating that at fixed Y_X , the masses (M_{500}) of clusters in Hicks et al. (2008) tend to be twice as high as in the LoCuSS sample. If the clusters in our sample have similarly low gas fractions compared to the LoCuSS sample, then the mass estimates we derive from the SZ scaling relation would be biased low. Our sample has a higher redshift range ($0.18 < z < 0.9$) than the LoCuSS sample (with a single cluster, A1689, in common to both samples), although the median redshift is not as high as in the Hicks et al. (2008) sample. We do not see any evidence for redshift evolution in the gas fraction biasing our results; the high redshift clusters are not more or less massive at a given Einstein radius than the lower redshift clusters. The lower redshift clusters lie within the redshift range probed by the LoCuSS sample from which we derive the scaling relation. Both the high and low redshift clusters span the Einstein radius and mass range of the complete sample, i.e., not all of the high redshift clusters are also high (or low) mass. One of the strong lensing clusters in our sample, RCS1J2319, is also in the sample studied by Hicks et al. (2008). They find that the gas fraction for this cluster is indeed low, and the X-ray derived hydrostatic M_{500} is about a factor of two larger than the mass we derive from SZ. X-ray measurements of f_{gas} for clusters in this sample would best resolve this issue.

A number of clusters in our sample have mass measurements given in the literature that differ from the masses inferred by the SZ scaling relation. For example, the weak lensing masses for A1703, SDSSJ1531, and SDSSJ2111 (scaling from M_{vir} to M_{500} , with measurements from Oguri et al. 2009), are systematically larger than the masses determined from the SZ scaling relation. Different mass observables are affected differently by properties such as alignment along the line of sight, and for strong lensing clusters that are preferentially aligned, larger masses are expected to be measured by weak lensing compared to SZ masses. Alternatively, if as discussed above the gas fractions for the strong lensing clusters were systematically lower than for the LoCuSS clusters, the masses we infer from the scaling relation could be underestimated.

3.3. Comparison with Previous Studies

We find that the Einstein radii are twice as large as expected for clusters of a given mass as inferred by SZ scaling relations, although the discrepancy has a significance of just 2σ . Previous studies have found that Einstein radii are larger than expected by a similar factor. Broadhurst & Barkana (2008a) also find that the Einstein radii for four clusters, two of which (A1689 and A1703) are also in our sample, are twice as large as expected. They interpret the significance of this result to be at 4σ , assuming each cluster to be an independent measurement and finding the probability that all four are discrepant with theoretical expectations by calculating the probability that each cluster is discrepant with Λ CDM predictions and then multiplying these probabilities together. Our larger sample of strong lensing clusters enables us to better model the sample selection effects, so although the size of the discrepancy between the observed and predicted Einstein radii is similar between the two studies, the significance is lower as we calculate it.

Richard et al. (2009) construct mass models from *Hubble Space Telescope* (*HST*) imaging of 10 low redshift clusters, adding to 10 other nearby strong lensing clusters from the literature, all selected as massive, X-ray luminous clusters. They find that the Einstein radii for their clusters are a factor of ~ 2 larger than predicted, but at a significance of 1.7σ , which they do not claim as a detection of a discrepancy.

Zitrin et al. (2011) conduct a similar study of 12 higher redshift ($z > 0.5$) X-ray selected clusters, constructing strong lensing models based on archival *HST* data. They find that the Einstein radii of their sample disagree with theoretical predictions by a factor of ~ 1.4 , even after accounting for lensing selection effects that could boost the lensing signal relative to samples selected by other methods. However, 8 out of the 12 clusters in their sample do not have spectroscopically measured redshifts for any of the lensed sources, resulting in considerable uncertainty in the Einstein radii for those clusters, as detailed therein.

While a direct comparison of these results is not straightforward because each study uses a different set of models and measures mass at a different radius, it is interesting to note that other studies using different methods to measure the clusters' masses also find that the measured Einstein radii tend to be larger than expected from theory, though sometimes at low significance.

4. SUMMARY

We measure the SZ effect for a sample of 10 galaxy clusters that were selected as strong lensing systems. Observations are conducted at 31 GHz using the SZA, and mass measurements are derived from these observations through a scaling relation based on weak lensing masses for the LoCuSS sample of clusters. Comparing these masses for the strong lensing selected clusters with their Einstein radii, derived from strong lensing mass modeling, provides information about their two-dimensional concentrations.

The data are modestly inconsistent with theoretical predictions, with evidence that the strong lenses tend to have Einstein radii that are a factor of two higher than their masses (as measured from SZ) would suggest according to these models. A Monte Carlo simulation indicates that the probability that a sample with the median difference from the theoretically expected Einstein radii is greater than or equal to that observed is 2.8%. This calculation accounts for the selection of large Einstein radius systems from the expected distribution of halos, thus improving upon the work done in a previous study of a smaller sample of strong lensing selected clusters (Broadhurst & Barkana 2008a).

We have investigated a number of systematic effects, including the possibility that the gas mass fraction of the strong lensing clusters is systematically lower than that of the LoCuSS clusters from which we derive the scaling relation, which would bias the SZ masses low. The LoCuSS clusters lie at lower redshift than most of the clusters in our sample, but we do not see any evidence that the high (low) redshift clusters have masses preferentially biased low (high) compared to the rest of our sample, indicating that the discrepancy between our observations and the expectations cannot be explained by simple gas fraction evolution. More sophisticated theoretical models of the strong lensing cluster population, perhaps moving toward full cosmological simulations that sample both the small scales and large volumes involved, with the addition of baryonic physics, may be needed to describe these observations.

This study is part of an ongoing program to acquire different mass proxies for strong lenses, including weak lensing and dynamical masses. Combining different mass proxies, with different sensitivities to the projection of line-of-sight structure, should enable more robust determinations of the distribution of mass in strong lensing clusters.

Support for this work is provided by NSF through award AST-0838187 and PHY-0114422 at the University of Chicago. Support for CARMA construction was derived from the Gordon and Betty Moore Foundation, the Kenneth T. and Eileen L. Norris Foundation, the James S. McDonnell Foundation, the Associates of the California Institute of Technology, the University of Chicago, the states of California, Illinois, and Maryland, and the National Science Foundation. Ongoing CARMA development and operations are supported by the National Science Foundation under a cooperative agreement, and by the CARMA partner universities. S.M. acknowledges support from an NSF Astronomy and Astrophysics Fellowship; C.G. and S.M. from NSF Graduate Research Fellowships; D.P.M. from NASA Hubble Fellowship grant HF-51259.01 Support for T.M. was provided by NASA through the Einstein Fellowship Program, grant PFO-110077.

Facility: CARMA

REFERENCES

- Abazajian, K. N., et al. 2009, *ApJS*, **182**, 543
 Andersson, K., et al. 2010, *ApJ*, submitted (arXiv:1006.3068)
 Bayliss, M., Hennawi, J. F., Gladders, M. D., Koester, B. P., Sharon, K., Dahle, H., & Oguri, M. 2011, *ApJS*, **193**, 8
 Bayliss, M., Wuyts, E., Sharon, K., Gladders, M. D., Hennawi, J. F., Koester, B. P., & Dahle, H. 2010, *ApJ*, **720**, 1559
 Bonamente, M., Joy, M. K., Carlstrom, J. E., Reese, E. D., & LaRoque, S. J. 2004, *ApJ*, **614**, 56
 Broadhurst, T. J., & Barkana, R. 2008a, *MNRAS*, **390**, 1647
 Broadhurst, T. J., Takada, M., Umetsu, K., Kong, X., Arimoto, N., Chiba, M., & Futamase, T. 2005, *ApJ*, **619**, 143
 Broadhurst, T., Umetsu, K., Medezinski, E., Oguri, M., & Rephaeli, Y. 2008b, *ApJ*, **685**, 9
 Duffy, A. R., Schaye, J., Kay, S. T., & Dalla Vecchia, C. 2008, *MNRAS*, **390**, L64
 Dunkley, J., et al. 2009, *ApJ*, **701**, 1804
 Fedeli, C., & Bartelmann, M. 2007, *A&A*, **461**, 49
 Gilbank, D. G., Gladders, M. D., Yee, H., & Hsieh, B. C. 2011, *AJ*, **141**, 94
 Gilbank, D. G., Yee, H. K. C., Ellingson, E., Hicks, A. K., Gladders, M. D., Barrientos, L. F., & Keeney, B. 2008, *ApJ*, **677**, 89
 Gladders, M. D., & Yee, H. 2000, *AJ*, **120**, 2148
 Hennawi, J. F., Dalal, N., Bode, P., & Ostriker, J. 2007, *ApJ*, **654**, 714
 Hennawi, J. F., et al. 2008, *AJ*, **135**, 664
 Hicks, A. K., Ellingson, E., Bautz, M., Cain, B., Gilbank, D. G., Gladders, M. G., Hoekstra, H., & Yee, H. K. C. 2008, *ApJ*, **680**, 1022
 Jing, Y. P., & Suto, Y. 2002, *ApJ*, **574**, 538
 Jullo, E., Kneib, J.-P., Limousin, M., Elíasdóttir, Á., Marshall, P. J., & Verdugo, T. 2007, *New J. Phys.*, **9**, 447
 Limousin, M., et al. 2007, *ApJ*, **668**, 643
 Limousin, M., et al. 2008, *A&A*, **489**, 23
 Mathis, H., Diego, J. M., & Silk, J. 2004, *MNRAS*, **353**, 681
 Meneghetti, M., Rasia, E., Merten, J., Bellagamba, F., Ettori, S., Mazzotta, P., Dolag, K., & Marri, S. 2010, *A&A*, **514**, 93
 Morandi, A., Pedersen, K., & Limousin, M. 2010, *ApJ*, **713**, 491
 Mroczkowski, T., et al. 2009, *ApJ*, **694**, 1034
 Muchovej, S., et al. 2007, *ApJ*, **663**, 708
 Nagai, D., Kravtsov, A. V., & Vikhlinin, A. 2007, *ApJ*, **668**, 1
 Narayan, R., & Bartelmann, M. 1997, arXiv:astro-ph/9606001
 Navarro, J. F., Frenk, C. S., & White, S. D. M. 1997, *ApJ*, **490**, 493
 Oguri, M., & Blandford, R. D. 2009, *MNRAS*, **392**, 930
 Oguri, M., Takada, M., Umetsu, K., & Broadhurst, T. 2005, *ApJ*, **632**, 841
 Oguri, M., et al. 2009, *ApJ*, **699**, 1038
 Okabe, N., Takada, M., Umetsu, K., Futamase, T., & Smith, G. P. 2010, *PASJ*, **62**, 811
 Richard, J., et al. 2009, *MNRAS*, **404**, 325

- Rozo, E., Nagai, D., Keeton, C., & Kravtsov, A. 2008, [ApJ](#), **687**, 22
- Smith, G. P., Kneib, J.-P., Smail, I., Mazzotta, P., Ebeling, H., & Czoske, O. 2005, [MNRAS](#), **359**, 417
- Torri, E., Meneghetti, M., Bartelmann, M., Moscardini, L., Rasia, E., & Tormen, G. 2004, [MNRAS](#), **349**, 476
- Wechsler, R. H., Bullock, J. S., Primack, J. R., Kravtsov, A. V., & Dekel, A. 2002, [ApJ](#), **568**, 52
- Wuyts, E., et al. 2010, [ApJ](#), **724**, 1182
- Zitrin, A., Broadhurst, T., Barkana, R., Rephaeli, Y., & Benítez, N. 2011, [MNRAS](#), **410**, 1939